


Strongly Reduced Thermal Conductivity of Supported Multilayer-Graphene Nanowires

S. Timpa¹,* J. Rastikian, S. Suffit¹, P. Lafarge¹, C. Barraud¹, and M.L. Della Rocca¹†
Laboratoire Matériaux et Phénomènes Quantiques, Université de Paris, CNRS, 75013 Paris, France

 (Received 2 March 2020; revised 27 April 2020; accepted 1 June 2020; published 20 July 2020)

The thermal properties of two-dimensional (2D) materials are of fundamental interest for energy recovery and electron cooling at the nanoscale. Exploring thermal transport in 2D systems is a challenging issue particularly in the substrate-supported architecture, which is the most relevant for applications. In this configuration, heat diffusion is strongly affected by thermal losses through the substrate and highly depends on interfacial properties. Here we investigate thermal transport of supported few-layer graphene nanowires by the Joule self-heating method in the high-temperature range ($400\text{ K} < T < 500\text{ K}$). This method is valuable for the substrate-supported sample configuration. By using a thick and rough oxide layer, we find that thermal losses through the substrate are reduced by almost 1 order of magnitude with respect to the expected theoretical values. Most importantly, we unveil an effective reduction of the thermal conductivity, with values as low as $40\text{ W m}^{-1}\text{ K}^{-1}$, comparable to reported values for supported graphene nanoribbons. Such a reduction can be induced by increased phonon scattering with the substrate and impurities in the system, which is inherent to the device fabrication. Our findings should stimulate research on alternative solutions for energy conversion at the nanoscale using graphene and other 2D materials when deposited on substrates.

DOI: [10.1103/PhysRevApplied.14.014056](https://doi.org/10.1103/PhysRevApplied.14.014056)

Two-dimensional (2D) materials, which are well studied in the fields of nanoelectronics and optoelectronics, have revealed intriguing properties for thermoelectric applications [1–3]. Graphene, one of the most-studied 2D materials, has high mobility and a large Seebeck coefficient [4–6] (up to $200\text{ }\mu\text{V K}^{-1}$ in hexagonal-BN supported devices), as well as very high thermal conductivity, reaching values up to $5000\text{ W m}^{-1}\text{ K}^{-1}$ [7] when suspended. Such a high value is a direct consequence of the strong bonding of light atoms and of the large phonon contribution to thermal transport [2,8]. These properties may provide a solution for electronic cooling at the nanoscale. The thermal properties of 2D materials are generally difficult to assess, and the suspended case is the most-explored configuration. Many different techniques are used to measure the thermal conductivity of 2D materials, the most-used ones being Raman optothermal spectroscopy [7,9], microresistance thermometry [10,11], the 3ω method [12], thermoreflectance [13], and electrical self-heating [14–16]. Each of them has different limitations, such as poor resolution, complex nanofabrication process, or limited sample dimensions. However, measurements on suspended 2D materials are not really relevant for applications. The ability to unveil the thermal and thermoelectric properties

of 2D materials in supported configurations is a major goal for applications. Measurement of the effective thermal conductivity of a supported low-dimensional material can be difficult, since thermal losses through the substrate dominate heat diffusion. Moreover, the interaction with the environment becomes a dominant factor for phononic thermal transport by typically reducing the thermal conductivity, k [17]. In the case of graphene, when lying on a substrate, phonon propagation is very sensitive to surface or edge perturbations [2,18]. A strong interface scattering of flexural phonon modes leads to a reduction of the thermal conductivity [19]. The thermal conductivity of single-layer graphene (SLG) supported on SiO_2 [9] was found to be reduced by almost 1 order of magnitude with respect to the suspended case, with a maximum value of $600\text{ W m}^{-1}\text{ K}^{-1}$ [11] at room temperature. By encasement of graphene between two SiO_2 layers [10], a further reduction was achieved, with values as low as $160\text{ W m}^{-1}\text{ K}^{-1}$. Measurements on supported graphene nanoribbons [20] show values down to $80\text{ W m}^{-1}\text{ K}^{-1}$ for 20 nm-wide samples. Recent theoretical work has also proved that controlling the surface state of the amorphous oxides underlying the device or the corrugation at the interface can drastically reduce thermal transport in graphene [18,21,22].

In this work, we apply the Joule self-heating method to simultaneously measure the thermal conductivity k and the

*salvatore.timpa@u-paris.fr

†maria-luisa.della-rocca@u-paris.fr

thermal losses per unit length g of supported multilayer-graphene (SMLG) nanowires (ten layers) and a supported bilayer-graphene (SBLG) nanowire. By carefully conceiving the device, we achieve a reduction of 1 order of magnitude in the predicted thermal losses and we find particularly low values of k . We use Si substrates covered by a thick and rough SiO₂ layer, over which SMLG nanowires are designed. A self-consistent fitting procedure, based on the resolution of the heat-diffusion equation, unveils k values on the order of 40–50 W m⁻¹ K⁻¹ and g values on the order of 0.05–0.15 W m⁻¹ K⁻¹ in the high-temperature range of 400 K < T < 500 K. By using the extracted g values, we find a reduced k value (approximately 100 W m⁻¹ K⁻¹) also for the SBLG nanowire fabricated on the same substrate. While showing reduced k , the SMLG and SBLG nanowires preserve good transport properties, with electrical conductivity σ on the order of 1×10^7 – 2×10^7 S m⁻¹. These observations demonstrate the relevance of a simple experimental method and device configuration that can be easily used to explore simultaneously thermal, electric, and thermoelectric properties of supported 2D material-based devices. At the same time, our findings revive research interest in the control of thermal properties of low-dimensional materials by well-thought-out device engineering.

I. EXPERIMENTAL METHODS

The Joule self-heating method is based on the resolution of the heat-transport equation in a nanowire crossed by a current in steady-state conditions [14–16]. In an optimized configuration, it appears as an alternative and easy method to measure the effective thermal conductivity of supported low-dimensional materials. This approach has the advantage of being implementable in device architectures compatible with thermopower and electrical conductivity investigations.

In the measurements, the graphene-based nanowire acts simultaneously as a heating element with homogeneous heat flux and an electrical thermometer. The small device dimensions guarantee that steady-state conditions by a constant heating current are reached on short timescales (less than 25 μ s). The applied method was used by Kodama *et al.* [14] in the case of supported metallic nanowires. It relies on the resolution of the heat-transport equation taking into account the thermal losses through the substrate:

$$kA \frac{d^2 T}{dx^2} + p[1 + \alpha(T - T_0)] - g(T - T_0) = 0, \quad (1)$$

where k is the nanowire thermal conductivity (including the electronic and lattice contributions), $A = Wh$ is the nanowire cross section, where W and h are the nanowire width and thickness, respectively, p is the applied electrical power per unit length, α is the temperature coefficient

of resistance (TCR), g is the term for heat losses through the substrate per unit length, and T_0 is the temperature of the environment. Thermal radiated losses from the surface can be neglected, being on the order of 0.14 W m⁻² K⁻¹ for graphene at room temperature [23].

The length scale to understand heat propagation in a supported nanowire is the so-called healing length [24], defined as $L_H = \sqrt{(kWh/g)}$. Numerical simulations have shown that for devices longer than $3L_H$, dissipation occurs almost entirely through the nanowire-substrate interface, while shorter devices benefit from substantial cooling through the metal contacts. As a consequence, for a “short” nanowire with $L < 3L_H$, L being the nanowire length, the temperature profile depends more on the thermal conductivity than on the thermal losses through the substrate. In contrast, for “long” nanowires ($L > 3L_H$), the temperature profile is more influenced by the thermal losses through the substrate than by the thermal conductivity. These observations allow one to clarify the procedure adopted to extract the k and g values in a supported nanowire configuration by self-heating, as pointed out in Ref. [14]. The relative resistance change $\Delta R/R_0$ due to the temperature increase of the nanowire induced by Joule heating can be calculated by solving Eq. (1) and is expressed as

$$\frac{\Delta R}{R_0} = \frac{\alpha p}{g - \alpha p} \left[1 - \frac{2}{mL} \tanh\left(\frac{mL}{2}\right) \right], \quad (2)$$

where $m = \sqrt{(g - \alpha p)/kA}$ and R_0 is the nanowire resistance when no heating occurs. The experimental evaluation of $\Delta R/R_0$ as a function of the applied power p is performed for short and long nanowires. First, we measure the resistance as function of the temperature of the environment for both nanowires to evaluate the TCR and calibrate the temperature response of the nanowires. This is done with a current intensity low enough to avoid self-heating. Second, the graphene-nanowire resistance variation due to self-heating is measured at higher currents. The fit of the experimental data to Eq. (2) is performed in a self-consistent way. Starting from a fixed value of k , we extract g by fitting the long-nanowire $\Delta R/R_0$ experimental data. The value of g obtained is used to estimate k by fitting the short-nanowire $\Delta R/R_0$ experimental data. The iterations are repeated until the k and g values converge.

II. DEVICE DESIGN

Thermal losses to the substrate are affected by different parameters, such as the interfacial thermal conductance G and the substrate thermal conductivity and thickness. In the case of graphene, the interfacial thermal conductance G can be strongly sample dependent. Different experimental investigations have reported values on the order of 100 MW m⁻² K⁻¹ for SLG and few-layer graphene [11,25] at 300 K, decreasing to 2 MW m⁻² K⁻¹

at 50 K in the case of exfoliated and encased graphene. Values of 50–100 MW m⁻² K⁻¹ have been found for carbon nanotubes [16]. It has also been estimated for large CVD-grown 2D materials flakes by Raman approach to be 27 MW m⁻² K⁻¹, 22 MW m⁻² K⁻¹, and 15 MW m⁻² K⁻¹ for SLG/SiO₂, MoS₂/SiO₂, and WSe₂/SiO₂ interfaces, respectively [26]. Recent results obtained by Tang *et al.* [23] demonstrated that increased substrate corrugation and the transfer technique used can lead to partially suspended zones of the SLG flake, leading to a reduction of G of several order of magnitude, down to 266 W m⁻² K⁻¹ in the SLG/SiO₂ case. Scanning-probe-microscopy measurements have confirmed that nonuniform graphene-substrate interface contact is typical of SLG exfoliated on SiO₂ over distances of a few tenths of nanometers [27,28]. The thermal losses per unit length, g , can be reduced by increasing the underlying oxide thickness, t_{ox} . Among the other parameters, the heat-spreading profile into the substrate depends on the nanowire width and the underlying-oxide thickness. Figure 1(a) shows a schematic of the different heat-spreading profiles in the cases of $W > t_{\text{ox}}$ and $W < t_{\text{ox}}$. In the latter case, lateral heat spreading plays an important role, and the thermal losses through the substrate per unit length, g , can be reduced with respect to the former case [20]. The general expression for g for $W < t_{\text{ox}}$ is given by Eq. (3):

$$g^{-1} = \left(\frac{\pi k_{\text{ox}}}{\log[6(t_{\text{ox}}/W + 1)]} + \frac{k_{\text{ox}}W}{t_{\text{ox}}} \right)^{-1} + \frac{1}{GW}, \quad (3)$$

where k_{ox} is the thermal conductivity of the underlying oxide layer and all the other terms have been defined before. By considering a G value on the order of 10 MW m⁻² K⁻¹, we chose the geometrical parameters of our devices fulfilling the condition $W < t_{\text{ox}}$. For $W = 300$ nm, $t_{\text{ox}} = 5$ μm, and $k_{\text{ox}} = 1.4$ W m⁻¹ K⁻¹, we estimate g to be approximately 0.7 W m⁻¹ K⁻¹. Such a value is almost 1 order of magnitude lower than what is theoretically expected in the opposite limit of $W > t_{\text{ox}}$, where uniform heat flux through the substrate is dominant.

Experimental investigations of the thermal losses through the substrate, g , in supported graphene are scarce in literature. Some indicative values are available for carbon nanotubes on SiO₂ and are on the order of 0.007–0.06 W m⁻¹ K⁻¹ as measured by scanning thermal microscopy [29], 0.03–0.11 W m⁻¹ K⁻¹ obtained by Raman thermometry [30], and 0.1–0.2 W m⁻¹ K⁻¹ extracted by breakdown method [24,31]. All these values are consistent with our estimation. Our discussion supports the idea that to minimize thermal losses through the substrate, graphene-based nanowires have to be fabricated over thick ($W < t_{\text{ox}}$) and rough SiO₂ layers. In addition, the choice of the nanowire length is fundamental to ensure the validity of the applied method. The thermal healing length can be calculated using a value of k equal

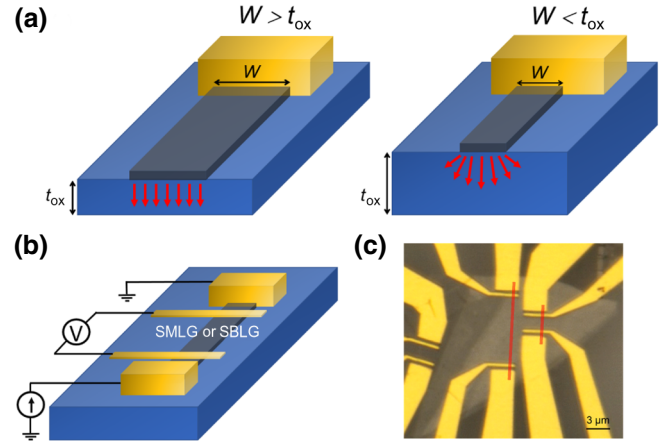


FIG. 1. (a) Heat spreading into the substrate in the cases $W > t_{\text{ox}}$ and $W < t_{\text{ox}}$. (b) Nanowire graphene device with electrical connections. (c) Optical image of the graphene flake before the etching with the etching mask.

to 600 W m⁻¹ K⁻¹, as extracted from the literature for supported graphene at 300 K, a g value as estimated by Eq. (3), and geometrical parameters (W, h, t_{ox}) corresponding to our fabricated devices. We find $L_H \sim 0.9$ μm, implying that the threshold length separating the short-long limit is equal to $3L_H \sim 2.7$ μm. Long nanowires are conceived with a length L greater than 3 μm and the short nanowires have a length smaller than 3 μm.

III. SAMPLE FABRICATION AND CHARACTERIZATION

Supported graphene nanowires are fabricated over Si substrates covered by a 5-μm-thick SiO₂ layer produced by plasma-enhanced CVD with a root-mean-square roughness of approximately 8 nm (as discussed later). The short and long nanowires have a width of 300 nm.

On the basis of the estimated value of $3L_H$, we fabricate a SMLG “short” nanowire with length $L_{\text{short}} = 1.8$ μm and a SMLG “long” nanowire with length $L_{\text{long}} = 9$ μm. This couple defines sample A. A second sample, sample B, has a unique SBLG nanowire of width $W = 300$ nm and length $L = 0.9$ μm. Figure 1(b) shows a schematic of our device configuration, where the graphene flake, represented by the gray layer, is connected to four metallic contacts for electrical transport measurements. The nanowire length L is defined as the inside edge-to-edge distance between the closest contacts. The graphene flakes are transferred with the hot pick-up technique over the substrate [32]. The four electrodes are successively patterned by electron-beam lithography and made by Ti(5 nm)/Au(100 nm) electron-gun evaporation. Finally, the graphene flakes are etched by reactive-ion etching with oxygen plasma (100-sccm O₂, 100 mTorr, 70 W for 60 s) to shape the intended nanowire geometries. Figure 1(c) shows an optical image of the

SMLG device before etching (sample A). The electrodes for the couple of short and long nanowires are fabricated intentionally as close as possible to each other on the same graphene flake to ensure similar nanowire properties. Etching is achieved with oxygen plasma through a resist mask of MaN-2401 defined by the red stripes in Fig. 1(c). Samples are finally rinsed in acetone and 2-propanol.

The number of layers in the graphene flakes is estimated by Raman spectroscopy in air at room temperature with a laser excitation wavelength of 514 nm, addressing in-plane vibrational modes. By comparing the peak intensity, shape and position of the 2D mode at 2700 cm^{-1} [Fig. 2(c)] with those in Raman spectra obtained from the literature for two, five, and ten layers [33], we can estimate the number of layers of the graphene flakes. In the case of sample A, there are ten layers, which corresponds to a thickness of approximately 3.5 nm, while for sample B there are two layers, corresponding to a thickness of approximately 0.7 nm.

AFM is used to investigate the surface morphology and roughness of the SiO_2 layer and of the overlying graphene flake. Figures 2(a) and 2(d) show 2D images for samples A and B, respectively, obtained at room temperature in atmosphere. For sample A, the SiO_2 surface has a root-mean-square roughness of $8 \pm 2\text{ nm}$ and a maximum peak-to-valley roughness of 20 nm. These parameters are calculated over average areas of approximately $1 \times 1\ \mu\text{m}^2$. The roughness reduces to $5 \pm 2\text{ nm}$ when it is measured on the graphene flakes. In the case of sample B, while the SiO_2 roughness remains unchanged, we measure a slightly

increased roughness on the graphene flake, equal to $6 \pm 1\text{ nm}$ over average areas of approximately $0.5 \times 0.5\ \mu\text{m}^2$. Representative line profiles are reported in Figs. 2(b) and 2(e) for the SMLG and SBLG nanowires, respectively. In both graphs, the solid gray line is a profile extracted over the SiO_2 surface, while the solid red (black) line is extracted over the graphene flake for sample A (sample B). The measured surface roughness hampers the estimation of the thickness of the graphene flakes by AFM. The AFM images also highlight suspended zones of the graphene flakes, revealing the nonconformal character at the interface.

All the electrical measurements are performed in a Nextron probe station under high vacuum ($P \sim 10^{-7}\text{ mbar}$). The nanowires and their metallic contacts are in thermal equilibrium with the underlying Si/SiO_2 substrate with large heat capacity. The substrate is anchored to an isothermal ceramic plate, whose temperature can be regulated with 0.1-K precision from 300 to 750 K. Since residuals of resist could be present on the surface [34], electrical current annealing is performed before measurements. The current is continuously swept between -2 and 2 mA under vacuum conditions at room temperature overnight. The maximum annealing current corresponds to an increase in temperature up to approximately 600 K. The thermal conductivity of supported graphene on rough SiO_2 substrates showing suspended zones has been measured close to that of suspended graphene. This value is found to decrease by repeated in-vacuum thermal annealing, which removes intercalated impurities, increasing

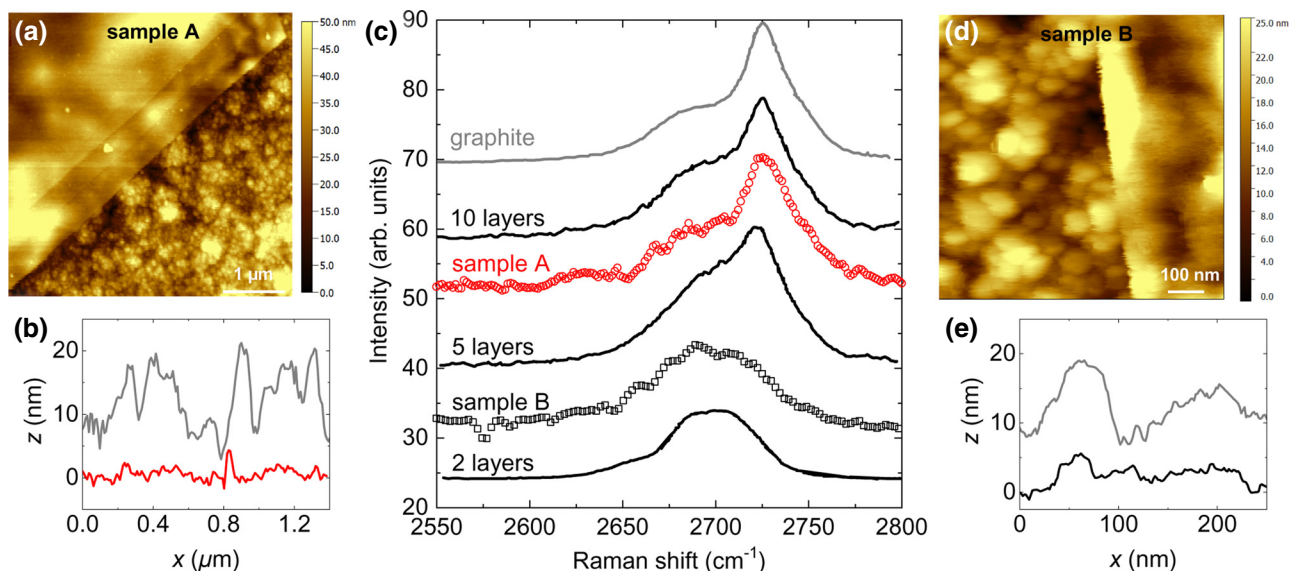


FIG. 2. (a) Two-dimensional AFM image of multilayer graphene over a $5\text{-}\mu\text{m}$ -thick SiO_2 surface (sample A). (b) AFM line profiles from sample A. The solid gray line is measured over the SiO_2 surface and the solid red line is measured over the graphene flake. (c) Raman spectra of samples A and B compared with literature spectra [33]. (d) Two dimensional AFM image of bilayer graphene over a $5\text{-}\mu\text{m}$ -thick SiO_2 surface (sample B) (e) AFM line profiles from sample B. The solid gray line is measured over the SiO_2 surface and the solid black line is measured over the graphene flake.

graphene-substrate conformity and interfacial scattering [18]. In our case the AFM characterization is performed before the annealing procedure. As a consequence, the graphene-substrate conformity during the transport experiments can be quite different from what is revealed by AFM.

The graphene-based-nanowire current-voltage characteristics $I(V)$ are measured in a four-probe configuration by current polarizing the nanowires while we measure the induced voltage drop [Fig. 1(b)]. The nanowire resistance is evaluated by the slopes of the $I(V)$ curves. The resistance calibration measurements are done by fixing the temperature of the sample holder in the micro probe station and by measuring the $I(V)$ curve at low bias ($|I| \leq 20 \mu\text{A}$). In this condition the $I(V)$ curves show a clear linear behavior, indicating that no detectable heating is induced. The procedure is repeated in a large temperature range (up to 575 K). The calibration procedure allows us to determine the TCR entering Eq. (1). After calibration, the sample holder is maintained at a fixed temperature and the sample is self-heated by sweeping the injected current I from $-I_{\text{heat}}$ to $+I_{\text{heat}}$, where I_{heat} is in the range from 300 to 400 μA depending on the nanowire. A maximum dissipated power on the SMLG and SBLG nanowires lower than 300 μW is allowed to guarantee a maximum temperature variation occurring in the nanowire below 30 K. Self-heating is revealed by a slightly nonlinear behavior in the $I(V)$ characteristics as the current increases. The resistance is computed as the derivative of the $I(V)$ curves, and the applied power p per unit length is defined as $p = I^2 R_0 / L_{\text{short (long)}}$. By repeating this measurement at different temperatures of the environment, we can experimentally estimate the $\Delta R/R_0$ relative variation. Electrical transport measurements are performed between 400 and 500 K. This temperature range is not often investigated but is relevant for commercial electronic devices working typically above room temperature. Moreover, few measurements of graphene-supported thermal conductivity are available in the literature in the high-temperature regime. Faugeras *et al.* [35] reported $k \sim 630 \text{ W m}^{-1} \text{ K}^{-1}$ for suspended single-layer graphene at 660 K with Raman optothermal technique. Dorgan *et al.* [36] used the electrical breakdown method on suspended SLG, finding $k \sim 310 \text{ W m}^{-1} \text{ K}^{-1}$ at 1000 K.

IV. RESULTS AND DISCUSSION

Figure 3 illustrates the result of the temperature calibration of the resistance for the short [Fig. 3(a)] and long [Fig. 3(b)] nanowire in the case of sample A. In both cases, high values of the electrical conductivity σ , on the order of 1×10^7 – $2 \times 10^7 \text{ S m}^{-1}$ can be extracted, revealing good electronic transport properties. Starting from room temperature, the experimental data show a different trend in the two cases. For the short nanowire, the resistance decreases

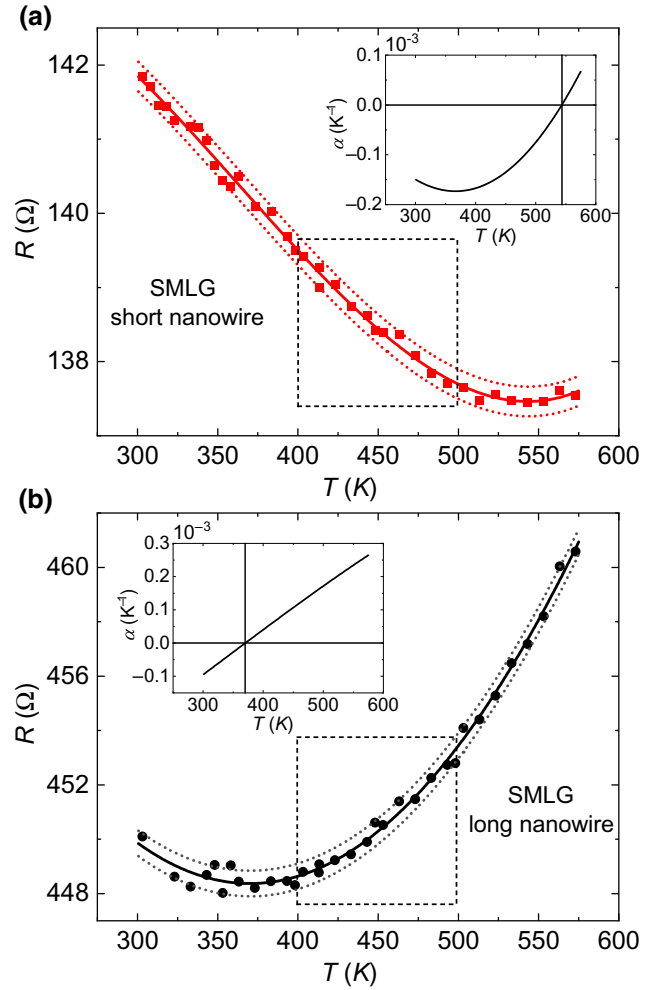


FIG. 3. Electrical resistance as a function of temperature for the long (a) and short (b) graphene nanowires (points) in sample A. The solid line represents the best experimental fit of the data. The dotted lines define the data dispersion over repeated measurements. The insets show the temperature coefficients α of the resistances for the two nanowires as a function of temperature.

until a minimum is reached around 550 K and subsequently it starts to rise. For the long nanowire, a resistance minimum is first seen around 350 K, followed by an increase at higher temperature. The two temperature dependencies of the nanowire resistances can be well described by cubic curves of the form $R(T) = AT^3 + BT^2 + CT + D$, where the quadratic term strongly dominates the cubic term ($B \sim 10^3$ – 10^4 A). The solid lines in Fig. 3 represent the best fit of the experimental data, and the dotted lines define the data dispersion obtained by repeated calibrations.

The quenching of graphene electrical resistance with temperature has been scarcely studied in the literature even though it is often observed. Shao *et al.* [37] measured decreasing behavior for single-layer and bilayer graphene in the temperature range $300 \text{ K} < T < 500 \text{ K}$, revealing a more pronounced reduction in the bilayer case. The same

observation has been reported for SLG from room temperature down to 10 K [38] and for suspended graphene nanoribbons in the temperature range $200 \text{ K} < T < 360 \text{ K}$ [39]. Nevertheless, these last studies are not focused on this particular aspect and do not comment on it. Few theoretical explanations are also available in the literature for the resistance decrease in SLG with temperature. One explanation relies on the dominant thermal generation of charge carriers accompanied by suppression of long-range disorder scattering [40]. As temperature increases, optical phonons contribution to electron scattering allows one to predict the existence of a resistance minimum. A second theoretical explanation ascribes the decreasing resistance behavior to the Friedel oscillations of the electron density around graphene defects, with strong sensitivity to their microscopic origin (e.g., structural defects, substitutional disorder, contact with the substrate). This means that the decreasing temperature dependence of graphene resistance should be particularly pronounced in the presence of a substrate [41]. Our experimental observations clearly show the existence of a minimum and the subsequent increasing of the SMLG nanowire resistance in the temperature range explored. The calibration curve for the SBLG nanowire in sample B is reported in Fig. 6(a) and also shows a decreasing behavior of the resistance as a function of the temperature, with no minimum revealed. This seems to indicate a length dependence of the position of the resistance minimum, with a shift toward lower temperatures as the length of the nanowire is increased. However, further investigations are necessary for a better understanding.

The insets in Fig. 3 show the TCR as extracted by the curve-fitting procedure for the short [Fig. 3(a)] and long [Fig. 3(b)] nanowires, defined as $\alpha(T) = [1/R(T)][dR(T)/dT]$. These temperature dependencies reveal that close to the temperature at which each SMLG nanowire has the resistance minimum, α approaches zero. As a consequence, to use Eq. (2) for self-heating data analysis, we restrict our experimental investigation to the temperature region $400 \text{ K} < T < 500 \text{ K}$, where both long and short nanowires are not affected by low values of α (dotted boxes in Fig. 3). For each measured temperature point, T^* , we consider $\alpha = \alpha(T^*)$ to apply the fitting procedure. Moreover, as discussed in Sec. III, restricting the dissipated power on the nanowires to values limiting a local temperature increase guarantees a correct approximation for data analysis when the $\alpha(T)$ dependence is used.

The relative variation of the SMLG nanowire's resistances, $\Delta R/R_0$, is measured as a function of the applied power p at different temperatures for a heating current ramping up to $\pm 400 \mu\text{A}$. Figure 4 shows two examples of data analysis at $T = 393 \text{ K}$ (red data) and $T = 453 \text{ K}$ (black data) for the long [Fig. 4(a)] and short [Fig. 4(b)] nanowires, respectively. The points are the measured experimental data and the dotted red and solid black

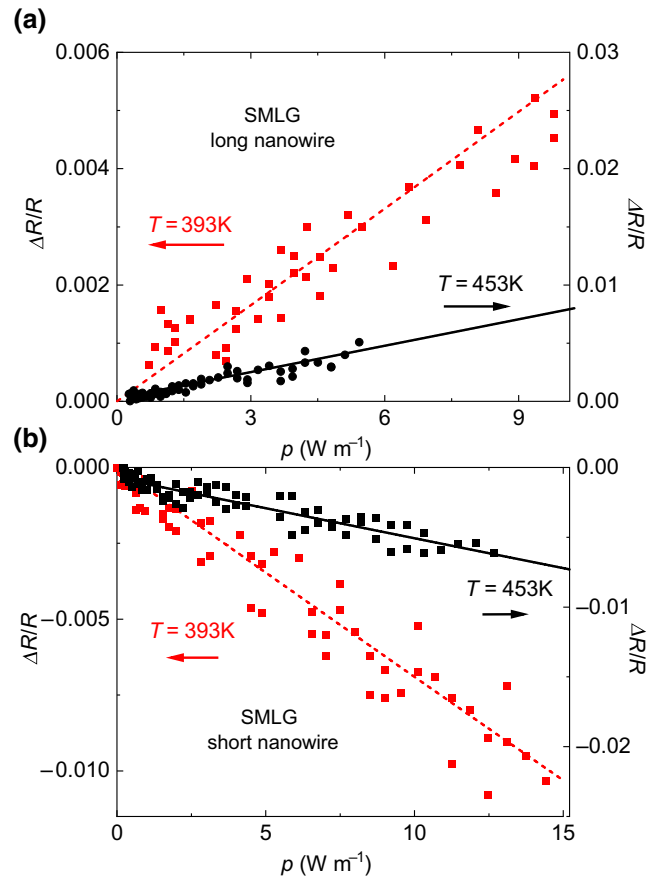


FIG. 4. (a) Relative variation of resistance for the long wire in sample A at $T = 393 \text{ K}$ (red squares) and $T = 453 \text{ K}$ (black circles) with the theoretical fit obtained by Eq. (2) (dotted and solid lines). (b) Same plot for the short nanowires in sample A.

lines are fitting plots resulting from Eq. (2). Convergence on the extracted k and g values is typically reached after ten iterations.

Figure 5(a) shows the complete set of k values extracted in the temperature range $400 \text{ K} < T < 500 \text{ K}$. We find particularly reduced values of the thermal conductivity in the temperature range explored. The extracted k values are on the order of $40 \text{ W m}^{-1} \text{ K}^{-1}$. The relatively large error bars result from the fitting procedure and reflect the difficulties to precisely evaluate the thermal conductivity. The results obtained do not allow us to define a tendency in the $k(T)$ behavior, but a reduction with respect to what is expected is evident in the whole temperature range explored. Even though we cannot discriminate the main physical mechanism inducing k reduction, some arguments can be discussed. Such low k values are comparable to what has been measured in the case of encased trilayer graphene [10]. In this particular example, the k reduction is due to induced defects and interactions between the outermost graphene layers and the encapsulating oxide layers. Two mechanisms are cited to

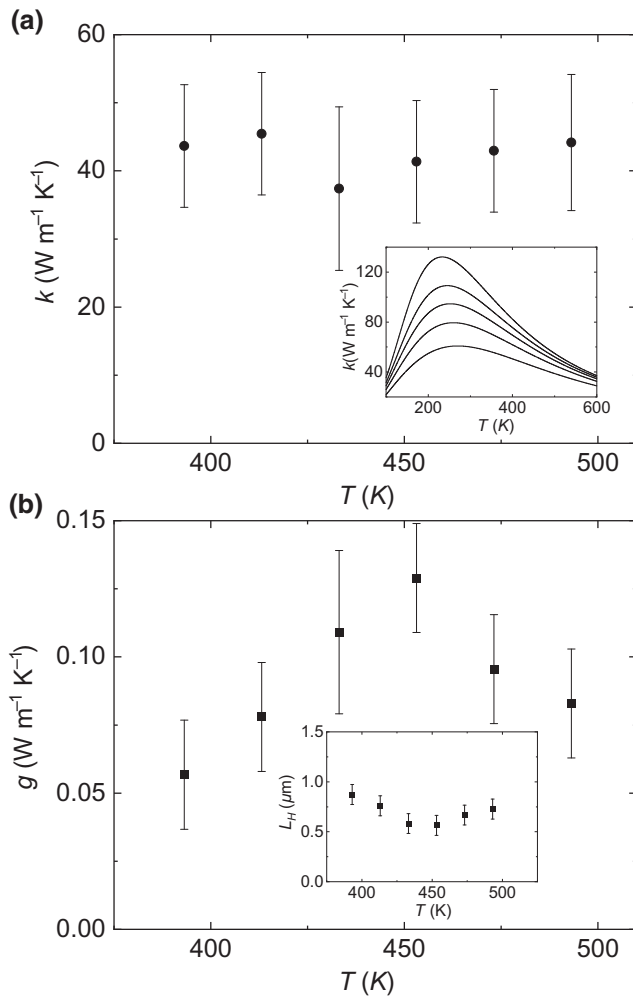


FIG. 5. (a) Thermal conductivity of SMLG nanowires in sample A as function of temperature. Error bars are derived from the fitting procedure. The inset shows a comparison of the extracted k values with the Callaway model [42] for increasing scattering with impurities. (b) Thermal losses through the substrate per unit length of SMLG nanowires in sample A as a function of temperature. The inset shows the thermal healing length estimated from the extracted k and g values as a function of the temperature.

explain the k reduction: phonon leakage into the low-sound-velocity oxide and additional phonon scattering by the inhomogeneous graphene-oxide interface. Similar k reduction has also been reported in supported graphene nanoribbons (below room temperature), where scattering with boundaries and with the substrate are dominant and limit the phonon diffusion [20]. In addition, the control of the in-plane thermal conductivity of supported graphene by varying the thermomechanical affiliation at the graphene-substrate interface has also been experimentally demonstrated. Repeated annealing enhances graphene-substrate conformity and interfacial scattering [18]. All this experimental evidence reported in the literature can apply also in our graphene-based nanowires and can be invoked

as a possible origin of k reduction. Theoretically, the temperature dependence of the thermal conductivity is expected to reach a maximum value at around room temperature. At higher temperature, significant *Umklapp* phonon scattering occurs, inducing a decreasing behavior [9–11,36]. The inset in Fig. 5(a) shows the theoretical $k(T)$ dependence based on the Callaway model, which is widely used in the literature to calculate the lattice thermal conductivity [42]. Within this description, the expression for the thermal conductivity is given by $k(T) = (k_B/2\pi^2\nu) (k_B T/\hbar)^3 \int_0^{\theta_D/T} \tau_c [x^4 e^x / (e^x - 1)^2] dx$, where k_B is the Boltzmann constant, ν is the graphene sound velocity, θ_D is the Debye temperature, and \hbar is the Planck constant. The model includes different phonon-scattering mechanisms, impurity (τ_I) and boundary (τ_B) scattering, the three-phonon normal process (τ_N), and the *Umklapp* process (τ_U), with an overall relaxation time, τ_c , given by the Matthiessen rule, $\tau_c = (\tau_I^{-1} + \tau_B^{-1} + \tau_N^{-1} + \tau_U^{-1})^{-1}$ [43]. The peak value of the thermal conductivity around room temperature is highly sensitive to crystal impurities and defects. By increasing the intensity of the impurity scattering terms, a strong $k(T)$ suppression can be theoretically predicted. Our results are qualitatively coherent with the prediction of the Callaway model. However, we cannot clearly identify which is the main scattering source for the reduction of the thermal conductivity experimentally detected. Clear insight into this question would require a detailed study of the thermal conductivity as a function of multiple parameters, such as controlled roughness and thickness of the SiO_2 layer, controlled introduction of impurities in the material, the nanowire's dimensions (length and width), and a wider temperature range. This is beyond the scope of the current work.

Figure 5(b) shows the values of the thermal losses through the substrate per unit length, g , extracted simultaneously to k . The values range between 0.05 and 0.15 $\text{W m}^{-1} \text{K}^{-1}$ in the temperature range explored. No significant temperature trend can be extracted. Anyway, the values obtained agree with what is estimated in Sec. II by Eq. (3), even though they are somewhat smaller. This is not surprising since it has been demonstrated that interfacial corrugation at the graphene- SiO_2 interface can reduce the interfacial thermal conductance by more than 1 order of magnitude [23]. Experimental investigations of the g parameter for supported graphene are scarce in the literature. The thermal conductance through the substrate can be highly sample dependent, and no systematic study as a function of the temperature has been performed to our knowledge. Our results are in agreement with the experimentally available values found for carbon nanotubes [16,24,29–31] and for single-layer graphene on SiO_2 [11,25,26]. Once the k and g values have been extracted, we can estimate the effective thermal healing length L_H of the fabricated SMLG nanowires to verify a

posteriori if they meet the “short-limit” and “long-limit” criteria. The inset in Fig. 5(b) shows the extracted L_H as a function of the temperature in the range explored. The values of L_H range between $0.5 \mu\text{m}$ and $1 \mu\text{m}$, matching, particularly for the highest values, the required condition.

In sample B (SBLG), only one measured nanowire of $0.9\text{-}\mu\text{m}$ -length fits the “short” condition. The experimental g , output of sample A, can be used in a first approximation for the analysis of the self-heating response of the SBLG nanowire in sample B. It has been revealed that the thermal conductance at the graphene-substrate interface does not change significantly across few-layer graphene (from one to approximately ten layers) [1,10,44]. This is because the thermal resistance between graphene and its environment dominates that between individual graphene sheets. The $R(T)$ dependence of the short SBLG nanowire is reported in Fig. 6(a), showing a monotonic decreasing behavior, together with the corresponding $\alpha(T)$ dependence in the inset. Similarly to sample A, we find good electronic transport properties with σ on the order of $1 \times 10^7 \text{ S m}^{-1}$.

The self-heating response of the SBLG nanowire in sample B analyzed by Eq. (2) is then computed with a g value of $0.09 \text{ W m}^{-1} \text{ K}^{-1}$, corresponding to the average value extracted for sample A, leaving only k as a free fit parameter. The result for the fitted k values as a function of the temperature is shown in Fig. 6(b). The thermal conductivity follows a trend equivalent to that for sample A, but with slightly higher values ranging between 80 and $120 \text{ W m}^{-1} \text{ K}^{-1}$. This result seems to indicate that the value of k can slightly vary depending on the local morphology and coupling to the underlying substrate. Previous experimental observations revealed increasing thermal conductivity as a function of the number of layers for supported and encased graphene [10,11,44], and an opposite trend in the suspended case [34,45]. We cannot conclude on the thickness dependence of k in our case. The estimation of the thermal healing length in this case is reported in the inset in Fig. 6(b), showing values that fulfill the “short” nanowire condition, justifying the data analysis used.

Our most relevant finding is that in both samples A and B, the extracted values of the thermal conductivity are lower than what has previously been observed in the literature by different approaches for supported few-layer graphene. Even though large error bars are present in our results, a decisive k suppression is evident. Scattering at the interface and the presence of residues related to the nanofabrication contribute to increased levels of impurities in the system, reducing further the thermal conductivity. Moreover, lateral-edge roughness and boundary effects can also contribute to the suppressed k behavior [46]. Annealing treatments can further contribute to decrease the graphene thermal conductivity since the interfacial phonon-scattering rate increases with increasing the graphene-substrate contact strength and conformity

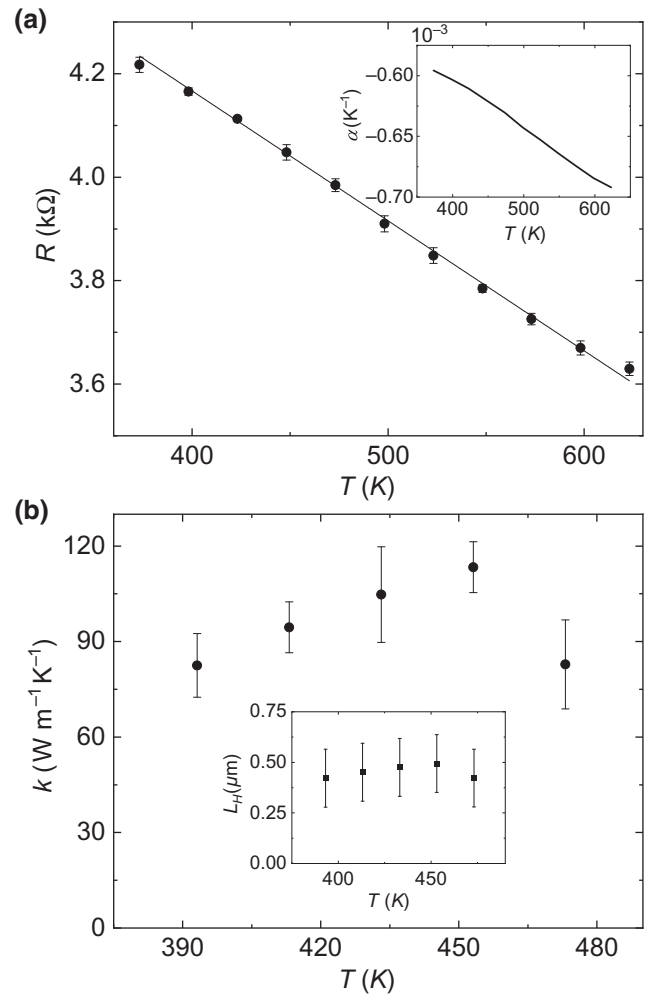


FIG. 6. (a) Electrical resistance as a function of temperature for the short SBLG nanowire (points) in sample B. The solid line represents the linear fit of the data. The inset shows the temperature coefficient α of the resistances for the nanowire as a function of temperature. (b) Thermal conductivity of SBLG nanowire in sample B as a function of temperature. Error bars are derived from the fitting procedure. The inset shows the thermal healing length estimated from the extracted k and g values as a function of temperature.

[11,18]. Finally, the high surface roughness of the substrate is likely to increase the thermal resistance at the interface, implying reduced thermal losses through the substrate too.

V. CONCLUSIONS

In this work we demonstrate that thermal transport in supported multilayer and bilayer graphene can be highly reduced in nanowires realized on rough SiO_2 surfaces. Increased phonon scattering with the substrate and the impurities can reasonably explain such suppression. Moreover, we demonstrate that thermal losses through the substrate can be minimized by increasing the thickness of the

oxide layer used, which further simplifies the measurement of the thermal conductivity in the supported case. Our results indicate that achieving better control of the graphene-substrate interface and the surface state could be a strategy to master thermal transport in supported graphene. Besides, we prove that the self-heating method can be implemented for a supported 2D-material device to achieve reliable information. The device configuration used to apply the self-heating method for investigating thermal transport properties is particularly suited for a complete *in situ* thermoelectric characterization of a wide class of low-dimensional materials. This is a striking point for applications. Our finding should promote a revival of interest in graphene for energy recovery at the nanoscale. Few-layer graphene can show simultaneously good electrical transport properties and degraded thermal ones, which can be particularly intriguing to conceive alternative solutions to face the heat waste problem in nanoscale systems.

ACKNOWLEDGMENTS

This work was funded partly by the 2DSPIN project from the Ville de Paris Emergence program. The Commissariat Général à l'Investissement d'Avenir and the Agence Nationale de la Recherche are also acknowledged for their financial support. We acknowledge Y. Gallais for Raman spectroscopy analysis, and P. Filloux and R. Duhamel for technical support in the clean room of the Laboratoire Matériaux et Phénomènes Quantiques (UMR 7162) at the University of Paris.

- [1] Y. Xu, Z. Li, and W. Duan, Thermal and thermoelectric properties of graphene, *Small* **10**, 2182 (2014).
- [2] E. Pop, V. Varshney, and A. K. Roy, Thermal properties of graphene: Fundamentals and applications, *MRS Bull.* **37**, 1273 (2012).
- [3] J. Wu, Y. Chen, J. Wu, and K. Hippalgaonkar, Perspectives on thermoelectricity in layered and 2D materials, *Adv. Electron. Mater.* **4**, 1800248 (2018).
- [4] Y. M. Zuev, W. Chang, and P. Kim, Thermoelectric and Magnetothermoelectric Transport Measurements of Graphene, *Phys. Rev. Lett.* **102**, 096807 (2009).
- [5] J. Duan, X. Wang, X. Lai, G. Li, K. Watanabe, T. Taniguchi, M. Zebarjadi, and E. Y. Andrei, High thermoelectric power factor in graphene/hBN devices, *Proc. Natl. Acad. Sci. USA* **113**, 14272 (2016).
- [6] M. Yoshida, T. Iizuka, Y. Saito, M. Onga, R. Suzuki, Y. Zhang, Y. Iwasa, and S. Shimizu, Gate-optimized thermoelectric power factor in ultrathin WSe_2 single crystals, *Nano Lett.* **16**, 2061 (2016).
- [7] A. A. Balandin, S. Ghosh, W. Bao, I. Calizo, D. Teweldebrhan, F. Miao, and C.-N. Lau, Superior thermal conductivity of single-layer graphene, *Nano Lett.* **8**, 902 (2008).
- [8] M. C. Schabel and J. L. Martins, Energetics of interplanar binding in graphite, *Phys. Rev. B* **46**, 7185 (1992).
- [9] W. Cai, A. L. Moore, Y. Zhu, X. Li, S. Chen, L. Shi, and R. S. Ruoff, Thermal transport in suspended and supported monolayer graphene grown by chemical vapor deposition, *Nano Lett.* **10**, 1645 (2010).
- [10] W. Jang, Z. Chen, W. Bao, C. N. Lau, and C. Dames, Thickness-dependent thermal conductivity of encased graphene and ultrathin graphite, *Nano Lett.* **10**, 3909 (2010).
- [11] J. H. Seol, I. Jo, A. L. Moore, L. Lindsay, Z. H. Aitken, M. T. Pettes, X. Li, Z. Yao, R. Huang, D. Broido, N. Mingo, R. S. Ruoff, and L. Shi, Two-dimensional phonon transport in supported graphene, *Science* **328**, 213 (2010).
- [12] Z. L. Wang, D. W. Tang, X. B. Li, X. H. Zheng, W. G. Zhang, L. X. Zheng, Y. T. Zhu, A. Z. Jin, H. F. Yang, and C. Z. Gu, Length-dependent thermal conductivity of an individual single-wall carbon nanotube, *Appl. Phys. Lett.* **91**, 123119 (2007).
- [13] J. L. Braun, D. H. Olson, J. T. Gaskins, and P. E. Hopkins, A steady-state thermoreflectance method to measure thermal conductivity, *Rev. Sci. Instrum.* **90**, 024905 (2019).
- [14] T. Kodama, W. Park, A. Marconnet, J. Lee, M. Asheghi, and K. E. Goodson, in *IEEE Intersociety Conference on Thermal and Thermomechanical Phenomena in Electronic Systems (ITHERM)* (San Diego, CA, 2012).
- [15] H. R. Barnard, E. Zossimova, N. H. Mahlmeister, L. M. Lawton, I. J. Luxmoore, and G. R. Nash, Boron nitride encapsulated graphene infrared emitters, *Appl. Phys. Lett.* **108**, 131110 (2016).
- [16] E. Pop, D. A. Mann, K. E. Goodson, and H. Dai, Electrical and thermal transport in metallic single-wall carbon nanotubes on insulating substrates, *J. Appl. Phys.* **101**, 093710 (2007).
- [17] L. Lindsay, D. A. Broido, and N. Mingo, Flexural phonons and thermal transport in multilayer graphene and graphite, *Phys. Rev. B* **83**, 235428 (2011).
- [18] H. G. Kim, K. D. Kihm, W. Lee, G. Lim, S. Cheon, W. Lee, K. R. Pyun, S. H. Ko, and S. Shin, Effect of graphene-substrate conformity on the in-plane thermal conductivity of supported graphene, *Carbon* **125**, 39 (2017).
- [19] Z.-Y. Ong and E. Pop, Effect of substrate modes on thermal transport in supported graphene, *Phys. Rev. B* **84**, 075471 (2011).
- [20] A. D. Liao, J. Z. Wu, X. Wang, K. Tahy, D. Jena, H. Dai, and E. Pop, Eric, Thermally Limited Current Carrying Ability of Graphene Nanoribbons, *Phys. Rev. Lett.* **106**, 256801 (2011).
- [21] A. France-Lanord, P. Soukiassian, C. Glattli, and E. Wimmer, Thermal Transport in Supported Graphene: Substrate Effects on Collective Excitations, *Phys. Rev. Appl.* **7**, 034030 (2017).
- [22] J. Han, Q. Liu, X. Li, J. Pan, L. Wei, Y. Wu, H. Peng, Y. Wang, G. Li, C. Chen, L. Xiao, J. Lu, and L. Zhuang, An effective approach for alleviating cation-induced backbone degradation in aromatic ether-based alkaline polymer electrolytes, *ACS Appl. Mater. Inter.* **7**, 2809 (2015).
- [23] X. Tang, S. Xu, J. Zhang, and X. Wang, Five orders of magnitude reduction in energy coupling across corrugated graphene/substrate interfaces, *ACS Appl. Mater. Inter.* **6**, 2809 (2014).

- [24] E. Pop, The role of electrical and thermal contact resistance for Joule breakdown of single-wall carbon nanotubes, *Nanotechnology* **19**, 295202 (2008).
- [25] Z. Chen, W. Jang, W. Bao, C. N. Lau, and C. Dames, Thermal contact resistance between graphene and silicon dioxide, *Appl. Phys. Lett.* **95**, 161910 (2009).
- [26] S. Vaziri, E. Yalon, M. Muñoz Rojo, S. V. Suryavanshi, H. Zhang, C. J. McClellan, C. S. Bailey, K. K. H. Smithe, A. J. Gabourie, V. Chen, S. Deshmukh, L. Bendersky, A. V. Davydov, and E. Pop, Ultrahigh thermal isolation across heterogeneously layered two-dimensional materials, *Sci. Adv.* **5**, eaax1325 (2019).
- [27] M. Ishigami, J. H. Chen, W. G. Cullen, M. S. Fuhrer, and E. D. Williams, Atomic structure of graphene on SiO₂, *Nano Lett.* **7**, 1643 (2007).
- [28] V. Geringer, M. Liebmann, T. Echtermeyer, S. Runte, M. Schmidt, R. Rückamp, M. C. Lemme, and M. Morgenstern, Intrinsic and Extrinsic Corrugation of Monolayer Graphene Deposited on SiO₂, *Phys. Rev. Lett.* **102**, 076102 (2009).
- [29] L. Shi, J. Zhou, P. Kim, A. Bachtold, A. Majumdar, and P. L. McEuen, Thermal probing of energy dissipation in current-carrying carbon nanotubes, *J. Appl. Phys.* **105**, 104306 (2009).
- [30] M. Steiner, M. Freitag, V. Perebeinos, J. C. Tsang, J. P. Small, M. Kinoshita, D. Yuan, J. Liu, and P. Avouris, Phonon populations and electrical power dissipation in carbon nanotube transistors, *Nat. Nanotechnol.* **4**, 320 (2009).
- [31] H. Maune, H.-Y. Chiu, and M. Bockrath, Thermal resistance of the nanoscale constrictions between carbon nanotubes and solid substrates, *Appl. Phys. Lett.* **89**, 013109 (2006).
- [32] F. Pizzocchero, L. Gammelgaard, B. S. Jessen, J. M. Caridad, L. Wang, J. Hone, P. Bøggild, and T. J. Booth, The hot pick-up technique for batch assembly of van der Waals heterostructures, *Nat. Commun.* **7**, 11894 (2016).
- [33] A. C. Ferrari, J. C. Meyer, V. Scardaci, C. Casiraghi, M. Lazzeri, F. Mauri, S. Piscanec, D. Jiang, K. S. Novoselov, S. Roth, and A. G. Geim, Raman Spectrum of Graphene and Graphene Layers, *Phys. Rev. Lett.* **97**, 187401 (2006).
- [34] W. Jang, W. Bao, L. Jing, C. N. Lau, and C. Dames, Thermal conductivity of suspended few-layer graphene by a modified T-bridge method, *Appl. Phys. Lett.* **103**, 133102 (2013).
- [35] C. Faugeras, B. Faugeras, M. Orlita, M. Potemski, R. R. Nair, and A. K. Geim, Thermal conductivity of graphene in corbino membrane geometry, *ACS Nano* **4**, 1889 (2010).
- [36] V. E. Dorgan, A. Behnam, H. J. Conley, K. I. Bolotin, and E. Pop, High-field electrical and thermal transport in suspended graphene, *Nano Lett.* **13**, 4581 (2013).
- [37] Q. Shao, G. Liu, D. Teweldebrhan, and A. A. Balandin, High-temperature quenching of electrical resistance in graphene interconnects, *Appl. Phys. Lett.* **92**, 202108 (2008).
- [38] S. Yiğen, V. Tayari, J. O. Island, J. M. Porter, and A. R. Champagne, Electronic thermal conductivity measurements in intrinsic graphene, *Phys. Rev. B* **87**, 241411 (2013).
- [39] H. Xie, L. Chen, W. Yu, and B. Wang, Temperature dependent thermal conductivity of a free-standing graphene nanoribbon, *Appl. Phys. Lett.* **102**, 111911 (2013).
- [40] F. T. Vasko and V. Ryzhii, Voltage and temperature dependencies of conductivity in gated graphene, *Phys. Rev. B* **76**, 233404 (2007).
- [41] V. V. Cheianov and V. I. Fal'ko, Friedel Oscillations, Impurity Scattering, and Temperature Dependence of Resistivity in Graphene, *Phys. Rev. Lett.* **97**, 226801 (2006).
- [42] J. Callaway, Model for lattice thermal conductivity at low temperatures, *Phys. Rev.* **113**, 1046 (1959).
- [43] M. G. Holland, Analysis of lattice thermal conductivity, *Phys. Rev.* **132**, 2461 (1963).
- [44] M. M. Sadeghi, I. Jo, and L. Shi, Phonon-interface scattering in multilayer graphene on an amorphous support, *Proc. Natl. Acad. Sci. USA* **110**, 16321 (2013).
- [45] S. Ghosh, W. Bao, D. L. Nika, S. Subrina, E. P. Pokatilov, C. N. Lau, and A. A. Balandin, Dimensional crossover of thermal transport in few-layer graphene, *Nat. Mater.* **9**, 555 (2010).
- [46] M.-H. Bae, Z. Li, Z. Aksamija, P. M. Martin, F. Xiong, Z.-Y. Ong, I. Knezevic, and E. Pop, Ballistic to diffusive crossover of heat flow in graphene ribbons, *Nat. Commun.* **4**, 1734 (2013).